Hindawi
Scientific Programming
Volume 2021, Article ID 7706782, 9 pages
https://doi.org/10.1155/2021/7706782

Research Article

Multilevel Clustering-Evolutionary Random Support Vector Machine Cluster Algorithm-Based Blood Oxygenation Level-Dependent Functional Magnetic Resonance Imaging Images in Analysis of Therapeutic Effects on Cerebral Ischemic Stroke

Zhili Zhang,[1] **Guo Cheng**,[2] **Guifang Liu**,[3] **and Gaixia Li**[4]

[1]*Department of Neurosurgery, Yantai Harbour Hospital, Yantai 264000, Shandong, China*
[2]*Department of Molecular Imaging, Affiliated Qingdao Central Hospital, Qingdao University, Qingdao 266042, Shandong, China*
[3]*Department of Radiology, Affiliated Qingdao Central Hospital, Qingdao University, Qingdao 266042, Shandong, China*
[4]*ECG Room, Qingdao Women and Children's Hospital, Qingdao 266000, Shandong, China*

Correspondence should be addressed to Gaixia Li; 1610947@tongji.edu.cn

Received 8 July 2021; Revised 3 September 2021; Accepted 6 September 2021; Published 4 October 2021

Academic Editor: Gustavo Ramirez

The study aimed to explore the relationship between cerebral ischemic stroke (CIS) and the patient's limb movement through the blood oxygenation level-dependent functional magnetic resonance imaging (BOLD-fMRI) based on multilevel clustering-evolutionary random support vector machine cluster (MCRSVMC). Specifically, 20 CIS patients were defined as the experimental group; another 20 healthy volunteers were defined as the control group. All subjects performed finger movement and verb association task. The performance of support vector machine (SVM) and MCRSVMC algorithm was compared and applied to functional magnetic resonance imaging (fMRI) of blood oxygen level in all subjects. The results showed that the average accuracy of MCRSVMC algorithm was significantly higher than that of support vector machine (86.75%, 65.84%; $P < 0.05$). The sensitivity of MCRSVMC algorithm was significantly higher than that of support vector machine (92.52%, 75.41%; $P < 0.05$). In addition, the specificity of MCRSVMC algorithm was significantly higher than that of support vector machine (86.39%, 68.24%; $P < 0.05$). When CIS patients performed finger exercise, the sensory motor areas on both sides were significantly activated, and the activated sensory motor areas on both sides were significantly bigger than the ipsilateral area. The activation rate of the left-sensory motor area (L-SM1) was 87.5%, the activation rate of the right-sensory motor area (R-SM1) was 25%, the activation rate of the left-side auxiliary motor area (L-SMA) was 62.5%, and the activation rate of the right-side auxiliary motor area (R-SMA) was 37.5%. In conclusion, the MCRSVMC algorithm proposed in this study is highly efficient and stable. BOLD-fMRI diagnosis of motor function in CIS patients is mainly related to compensation around the lesion, which occurs on the healthy side after recovery.

1. Introduction

Cerebral ischemic stroke (CIS) refers to brain tissue ischemia caused by cerebrovascular diseases, accompanied by neuronal necrosis arising from a series of complex ischemic cascade reactions [1]. It is the most common type of cerebrovascular diseases, accounting for up to 87%, which seriously endangers people's health [2]. It is characterized by high morbidity, high disability, high mortality, and high recurrence rate. Although the pathogenesis of CIS is different, the key to early treatment is to recanalize the blood vessels as soon as possible, so as to promote the recovery of blood flow in the ischemic penumbra area, and save the non-necrotic brain cells in time [3–5]. CIS patients are most prone to motor dysfunction. The damage to upper motor neuron function causes motor dysfunction. As a result, the

high center loses control of the motor system, so that the motor reflex of the subcortical center is released, and the motor system is abnormal [6].

In the rehabilitation of motor function, the reorganization of brain function plays a very important role. However, it is not clear which area of the cortex causes the difference in recovery. Blood oxygen levels depending on functional magnetic resonance imaging (BOLD-fMRI) can non-invasively detect the activity in the brain. It detects the activity in the central nervous system to observe the brain cortex activity caused by external stimuli [7–9]. Support vector machine (SVM) is a commonly used pattern classification algorithm. Compared with other algorithms, SVM can be applied to small datasets and non-linear mapping and has the advantages of rigorous mathematical logic and strong generalization ability [10]. It is widely used in neurological diseases and can be applied to detect abnormal patterns of brain function in high-dimensional data of functional magnetic resonance imaging (fMRI). In this study, based on functional magnetic resonance imaging, a multilevel clustering-evolutionary random support vector machine cluster (MCRSVMC) was innovatively proposed. MCRSVMC algorithm is an integrated technology based on SVM. Taking advantage of the advantages of SVM in fMRI data, a large number of SVM-based classifiers can be constructed to form clusters by randomly selecting some features and samples, and finally the test samples are classified by equal voting. Pruijm et al. [11] used MCRSVMC algorithm to process MRI images, combined with clustering evolution on the basis of multiple support vector machine classifiers, and finally improved the classification performance of the model. Blood oxygen level-dependent functional magnetic resonance imaging based on multilevel clustering evolution and stochastic support vector machine clustering can realize the selection of features and further detect abnormal brain regions of ischemic stroke [12].

In this study, multiple SVMs were combined, then clustering evolution was applied to increase the difference of independent learners in the cluster, and finally a random SVM cluster with high classification accuracy was obtained. The MCRSVMC-based BOLD-fMRI was used to evaluate the efficacy of CIS patients, aiming to conduct in-depth research on the brain functional areas of CIS and provide a basis for the treatment of CIS-induced motor dysfunction.

2. Materials and Methods

2.1. Research Subjects. In this study, 20 CIS patients treated at the hospital from January 15, 2019, to December 20, 2020, were defined as the experimental group, with 9 males and 11 females, with an average age of 48.26 ± 10.47 years. Another 20 healthy volunteers were selected as the control group, 12 males and 8 females, with an average age of 45.38 ± 11.32 years old, no neurological diseases, not engaged in the computer industry, and normal finger movement functions. The study has been approved by the Medical Ethics Committee of the hospital, and the patients and their families understood the situation of the study and had signed an informed consent form.

The subjects were selected as per the following inclusion criteria: (I) first occurrence of cerebrovascular accident, with onset time within 1–16 days; (II) patients with no history of neurological diseases; (III) not in computer-related professions; (IV) patients with no other abnormalities in body sensation except motor dysfunction; and (V) patients whose vital signs were normal.

Exclusion criteria: (1) patients with a history of cerebral infarction or cerebral hemorrhage; (2) patients with obvious disturbance of consciousness and neurological function; (3) patients with impairment in comprehension; and (4) patients unable to cooperate with the investigation normally.

2.2. Observation Indicators. The statistical function of SPM (Salford Systems, USA) was used for group analysis to obtain average images of group data and the accurate total cortical activation data of individual observation intuitively and quickly. In addition, the active areas of interest of SPM were used to analyze the activation curve of brain death, which intuitively reflected the relationship between the activated areas and the stimulus.

2.3. Conventional MRI and BOLD-fMRI Examination Methods. Achieva X-series 3.0 T magnetic resonance imager (Philips, the Netherlands) was used for scanning. Before the scan, the patient lied on his back for 5–10 minutes. The multichannel phased array head collar was used. First, the conventional head plain scan, T1WI transverse scan, and T2WI transverse scan were performed, with slice thickness of 5 mm, repetition time of 300 ms, echo time of 20 ms, and matrix of 320×192.

During fMRI scan, in addition to passively accepting finger movement, the patients should keep still as much as possible. Then, the structure scan and the finger-to-finger movement of the affected upper limb were conducted. The whole brain three-dimensional structure imaging scan adopts T1WI sequence, with layer thickness of 1.3 mm, repetition time of 3000 ms, echo time of 10.5 ms, matrix of 256×192, flip angle of 15°, and imaging frame number of 300. BOLD-fMRI uses T2WI gradient echo-plane echo imaging sequence, with slice thickness of 5 mm, repetition time of 3000 ms, echo time of 40 ms, maximum field of view of $240\,\text{mm} \times 240\,\text{mm}$, matrix of 256×256, voxel size of $2.4 \times 2.4 \times 1.8$ mm, phase encoding direction of AP, flip angle of 90°, scanning time of 4 min, number of acquisition layers of 80 layers/frame, 3 s/frame, and number of imaging frames of 2400 frames.

Before the experiment, patients in the experimental group need to understand the purpose, method, and content of the experiment, as well as the method, strength, amplitude, and frequency of the training exercise. The training was repeated 4 times in a sequence from rest to stimulation. In the resting state, the patient kept still and did not move; during stimulation, the patient performed a unilateral hand-to-finger movement, that is, a match of the thumb and the other four fingers. The frequency is 1 time/second, and the mode, amplitude, and frequency of the finger movement are kept consistent. The stimulation and resting lasted for 40 s,

respectively. Volunteers in the normal control group underwent fMRI examinations for verb association and picture tasks.

2.4. MCRSVMC-Based Algorithm. In this study, clustering algorithm is used to select SVM with higher accuracy as the cluster representative to select the model. Suppose there is a dataset $D = \{X_1, X_2, \ldots, X_k\}$ and individual learners, SVM_1, SVM_2, SVM_3,...SVM_n; the SVM learners are classified as follows:

$$G_i(x) = \begin{cases} 1, & \text{SVM classified correctly} \\ 0, & \text{SVM classification error} \end{cases}, R = \sum_{L=1}^{K} F\left(G_{(L,i)} = G_{(L,j)} = 1\right), \tag{1}$$

where k represents the number of samples in the dataset, R represents the number of correctly classified data by SVM_i and SVM_j, and $F(*)$ represents the indicator function.

$$W = \sum_{L=1}^{K} F\left(\left(G_{(L,i)} = 1\right) \wedge \left(G_{(L,j)} = 0\right)\right), \tag{2}$$

where W represents the number of samples in the dataset that are correctly classified by SVM_i and incorrectly classified by SVM_j, k represents the number of samples in the dataset, and $F(*)$ represents the indicator function.

$$S = \sum_{L=1}^{K} F\left(\left(G_{(L,i)} = 0\right) \wedge \left(G_{(L,j)} = 1\right)\right), \tag{3}$$

where S represents the number of samples in the dataset that are classified incorrectly by SVM_i and correctly classified by SVM_j, k represents the number of samples in the data set, and $F(*)$ represents the indicator function.

$$T = \sum_{L=1}^{K} F\left(G_{(L,i)} = G_{(L,j)} = 0\right), \tag{4}$$

where T represents the number of samples that are incorrectly classified by both SVM_i and SVM_j, k represents the number of samples in the dataset, and $F(*)$ represents the indicator function.

In this study, dataset D is randomly divided into combination set A and test set B. The combination set A is continuously divided into training set A_{train} and verification set $A_{\text{verification}}$. When training the learner, the set A is used to divide the training set and the validation set, thereby increasing the diversity of the learner. The set B is used to determine the generalization ability of MCRSVMC algorithm. Figure 1 shows a flowchart of the MCRSVMC algorithm.

2.5. Simulation Experiment Design. The performance of the MCRSVMC algorithm is evaluated factoring in accuracy, sensitivity, and specificity.

$$C = \frac{\text{TP} + \text{TN}}{\text{TP} + \text{FP} + \text{FN} + \text{TN}}, \tag{5}$$

where the accuracy rate C represents the number of samples correctly classified in all samples, TP represents true positives, TN represents true negatives, FP represents false positives, and FN represents false negatives.

$$Sensitivity = \frac{\text{TP}}{\text{TP} + \text{FN}}, \tag{6}$$

where sensitivity represents the number of samples that are correctly classified among all positive samples, TP represents true positives, and FN represents false negatives.

$$Specificity = \frac{\text{TN}}{\text{FP} + \text{TN}}, \tag{7}$$

where specificity represents the number of correctly classified samples among all negative samples, TN represents true negatives, and FP represents false positives.

As for the pathogenesis of CIS, in the study, the MCRSVMC algorithm is used to classify to search the abnormal characteristics in the brain. First, it is necessary to find the optimal number of base classifiers of MCRSVMC, then feature extraction is performed, and finally important features and optimal feature subsets are found. The corresponding brain area is identified through the feature, and the frequency of the brain area is counted.

2.6. Statistical Method. The data were processed by SPSS19.0, the measurement data were expressed as mean ± standard deviation ($\overline{x} \pm s$), and the count data were expressed as percentage (%). Pairwise comparison used analysis of variance. Statistical parameter mapping (SPM) was used to analyze brain function imaging data. $P < 0.05$ was the threshold for significance.

3. Results

3.1. Performance Comparison of Two Models. Figure 2 shows the comparison results of the two models. In this research, the performance of support vector machine and MCRSVMC algorithm was compared. The number of base classifiers of both models was set to 400. The average accuracy of MCRSVMC algorithm (86.75%) was significantly higher than that of support vector machine (65.84%), and the difference was statistically significant ($P < 0.05$). The sensitivity of MCRSVMC algorithm (92.52%) was significantly higher than that of support vector machine (75.41%), and the difference was statistically significant ($P < 0.05$). The specificity of MCRSVMC algorithm (86.39%) was significantly higher than that of support vector machine (68.24%), and the difference was statistically significant ($P < 0.05$). In the images processed by MCRSVMC algorithm, the areas of red and yellow gradient increased, indicating that MCRSVMC algorithm could significantly enhance the diagnosis of abnormal brain regions.

3.2. fMRI Results in Healthy Control Group. Table 1 shows the fMRI-activated brain regions of the healthy control group. In the healthy control group, the main brain areas

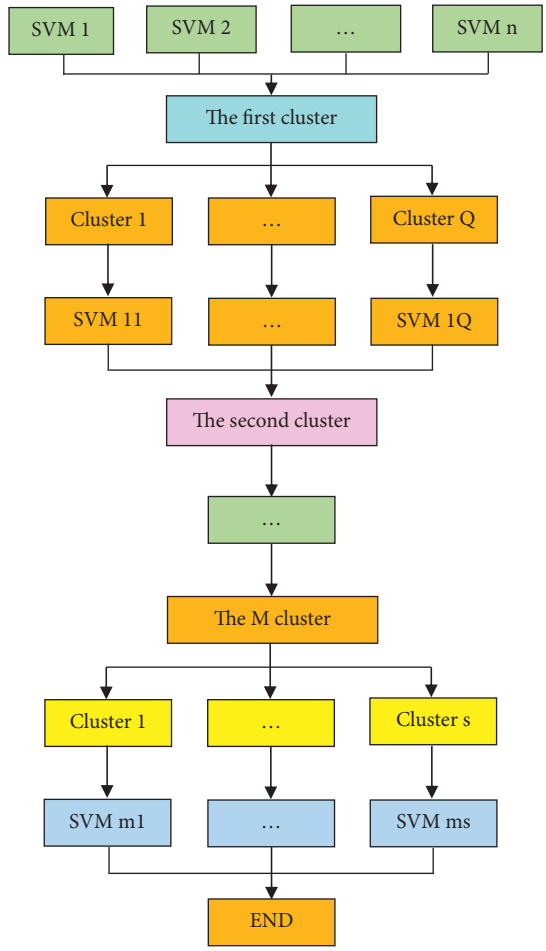

Figure 1: A flowchart of the MCRSVMC algorithm.

activated by verb association task were the auxiliary motor area (BA6) with coordinates of (0, 15, 52), right Broca region (BA45) with coordinates of (32,32,4), right anterior cingulate gyrus (BA32) with coordinates of (10, 20, 25), and the left fusiform gyrus (BA37) with coordinates of (−45, −55, −18). The main brain areas activated by the image naming task were the right visual cortex (BA18) with coordinates of (15, −82, −10), the left fusiform gyrus (BA35) with coordinates of (−36, −43, −16), and the left Broca region (BA45) with coordinates of (−5, 25, 5).

3.3. BOLD-fMRI Results of Brain Area Activated by Finger Movement in Patients with CIS. There was a significant difference in the activated brain areas by finger movement between normal people and CIS patients. Obviously, in the CIS patients, the precentral gyrus dominance area was significantly activated (BA4); the left precentral gyrus (BA2) and the postcentral gyrus dominance area of the hand (BA7) were activated by small clusters; and the right paracentral lobules (BA5), angular gyrus (BA19), cerebellar dentate nucleus (BA39), left superior frontal gyrus (BA8), paracentral lobules (BA5), and angular gyrus (BA1) were activated by patches. The brain function inhibition areas were mainly distributed in the left limbic system of the brain, including the left cingulate gyrus (BA32), the left hook gyrus (BA35), the caudate nucleus (BA20), and the right parahippocampal gyrus (BA28). The cerebral cortex includes the left medial prefrontal lobe (BA20), with small activation clusters (Figure 3).

Figure 4 shows the activated brain areas by the finger movement. The image processed by statistical parameter mapping mainly displayed the sensory motor area (SM1) and the lateral auxiliary motor area (SMA).

Figure 5 shows cerebral cortex activation. When CIS patients conducted finger exercise, the sensory motor areas on both sides were significantly activated, and the activated areas were significantly bigger than the ipsilateral area.

3.4. Brain Activation Rate. Figure 6 shows the activation rate of brain regions in CIS patients. The activation rate of each brain area was calculated based on cortical activation perspective view combined with the coordinate of each activation area. The results showed that the activation rate of the left-sensory motor area (L-SM1) was 87.5%, and the activation rate of the right-sensory motor area (R-SM1) was 25%; the activation rate of the left-side auxiliary motor area (L-SMA) was 62.5%, and the activation rate of the right-side auxiliary motor area (R-SMA) was 37.5%.

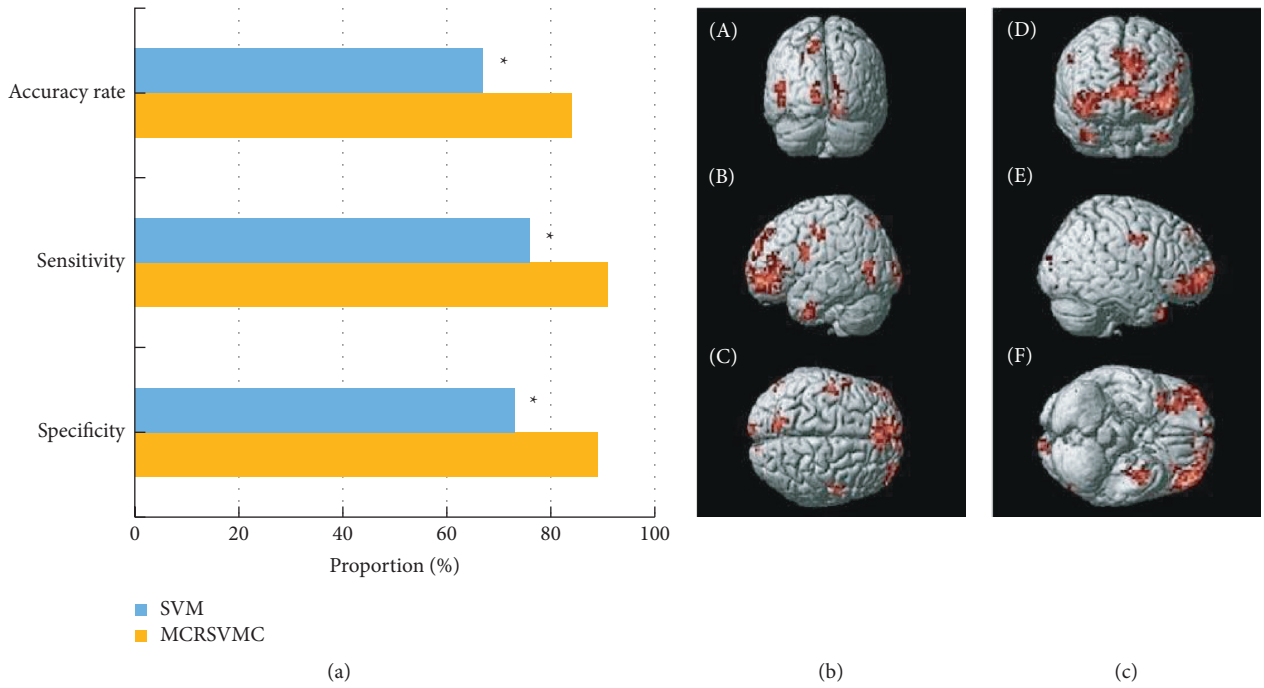

Figure 2: Comparison results of the two models: (a) performance comparison result; (b) support vector machine processing results—(A) coronal, (B) sagittal, and (C) axial; (c) results of MCRSVMC treatment—(D) coronal, (E) sagittal, and (F) axial. Note: ∗ indicates that the difference was statistically significant compared with MCRSVMC algorithm ($P < 0.05$).

Table 1: fMRI-activated brain regions in healthy control group.

Task	Anatomy	Brodmann area (BA)	Coordinate			Voxel
			X	*Y*	*Z*	
Verb association	Auxiliary exercise area	6	0	15	52	56
	Right Broca area	45	32	32	4	75
	Right anterior cingulate gyrus	32	10	20	25	35
	Left fusiform gyrus	37	−45	−55	−18	34
Picture naming	Right visual cortex	18	15	−82	−10	1285
	Left fusiform gyrus	35	−36	−43	−16	236
	Left Broca area	45	−5	25	5	15

3.5. BOLD-fMRI of CIS Patients before and after Treatment. The activation of the cerebral cortex of the patient was observed, and it was found that activated areas of CIS patients in the acute phase were mainly around the stroke area and the patient's parietal lobe. Some patients showed mild activation of the occipital lobe, temporal lobe, and cuneiform lobe, as shown in Figure 7. After treatment, the main manifestations of the patients were cerebral hemisphere excitation, and individual patients showed cortex excitation in the sensorimotor area, as shown in Figure 8.

4. Discussion

The BOLD-fMRI currently used can stimulate the corresponding functional activities of brain regions according to the movements of peripheral organs and sensory movements, and the changes in the signal intensity of brain tissue observed by MRI images can directly reflect the changes in brain tissue function [13–15]. For patients with ischemic stroke, BOLD-fMRI can visually reflect the characteristics of brain functional restructuring in patients and observe the recovery function of limbs and the activation of brain-related cortex [16]. When the CIA patients performed finger movement and verb associations, the cerebral cortex controlled by the related motor functions will be excited, causing increased metabolism and oxygen consumption. Also, blood vessels expand, and local blood flow increases, which will lead to the increase of local oxygen hemoglobin. BOLD-fMRI combined with conventional MRI can clearly observe the location, intensity, and range of excitement in the cerebral cortex caused by exercise [17–19].

BOLD-fMRI is a neuroimaging technology with no radiation exposure, non-invasiveness, and high safety. It provides effective data support for the study of human brain cognitive function. In this study, based on the characteristics of BOLD-fMRI images, the MCRSVMC algorithm was proposed. It established SVM classifier using a random sampling method and increased the diversity of SVM by

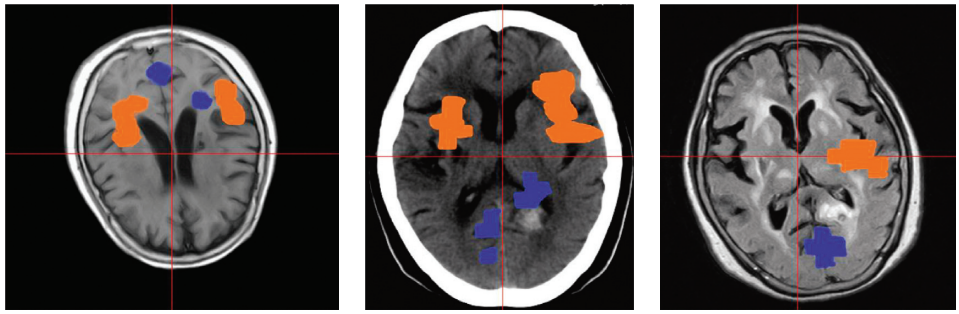

(a) (b) (c)

Figure 3: Registration module for statistical parameter mapping preprocessing. (a) Patient who was male, 48 years old, and had significantly activated the dominant area of the central anterior gyrus of the affected side. (b) Patient who was female and 46 years old (her right paraventricular lobule was activated in sheet form). (c) Patient who was male and 51 years old, with small activation cluster of right parahippocampal gyrus. Note: blue indicated a decrease in the BOLD signal, while orange indicated an increase in the BOLD signal.

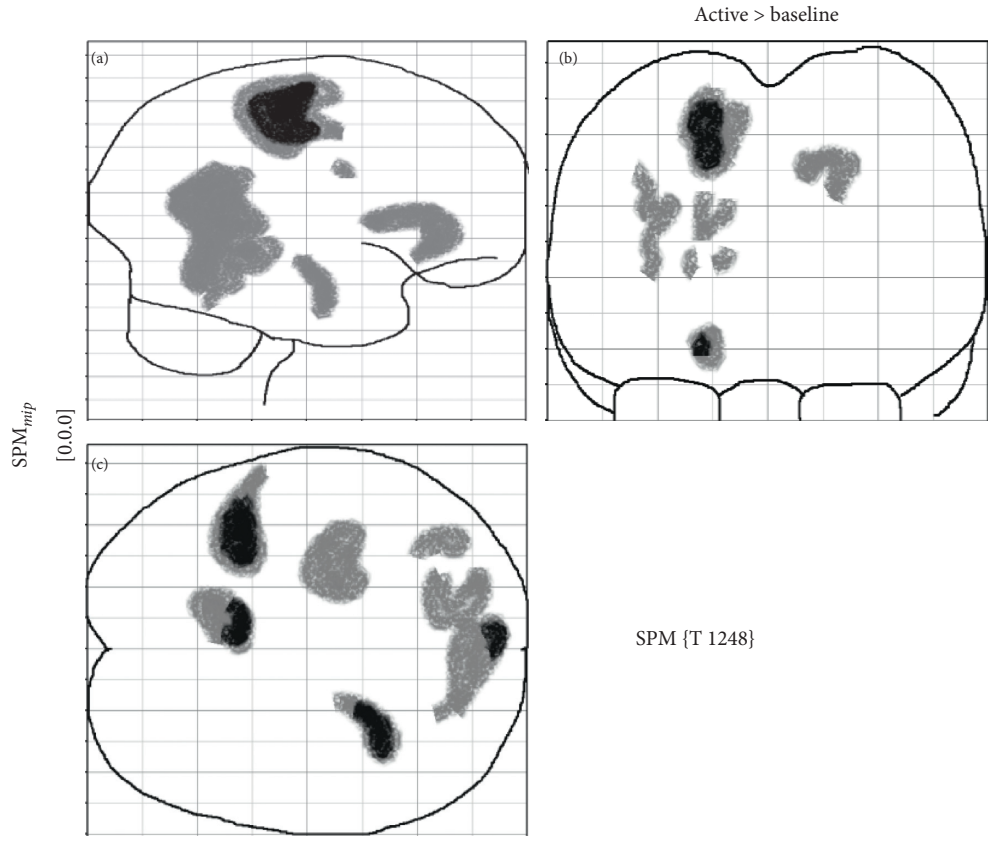

Figure 4: The activated brain areas by the finger movement: (a) sagittal position; (b) coronal position; (c) transverse position. Note: black indicated increased signal in activated brain areas, while gray indicated decreased signal.

introducing a clustering algorithm [20]. The results showed that the average accuracy of MCRSVMC algorithm (86.75%) was significantly higher than that of random forest (72.36%) and SVM (65.84%) ($P < 0.05$); the sensitivity of MCRSVMC algorithm (92.52%) was significantly higher than that of random forest (72.34%) and SVM (75.41%) ($P < 0.05$); and the specificity of MCRSVMC algorithm (86.39%) was significantly higher than that of random forest (73.45%) and SVM (68.24%) ($P < 0.05$). Taken together, it suggested that the MCRSVMC algorithm was highly efficient and stable.

The activated brain areas in the healthy control group during the verb association task mainly included auxiliary motor area, right Broca area, right anterior cingulate gyrus, and left fusiform gyrus, indicating that the verb association task mainly activated the frontal parietal cortex, and the bilateral occipital area was activated by a small area [21–23]. The

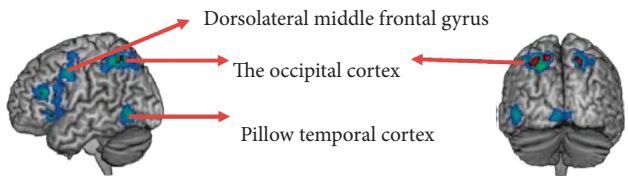

Figure 5: The cerebral cortex activation in patients with CIS.

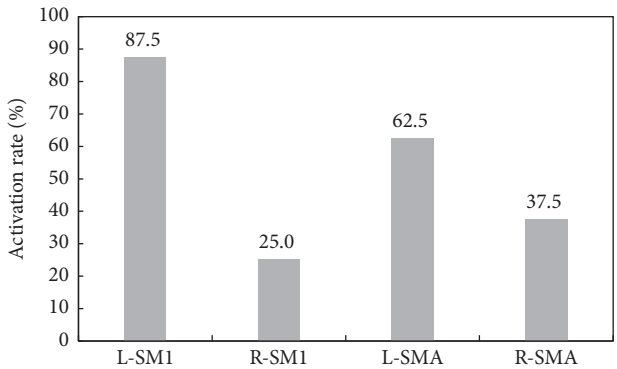

Figure 6: Activation rate of each brain area.

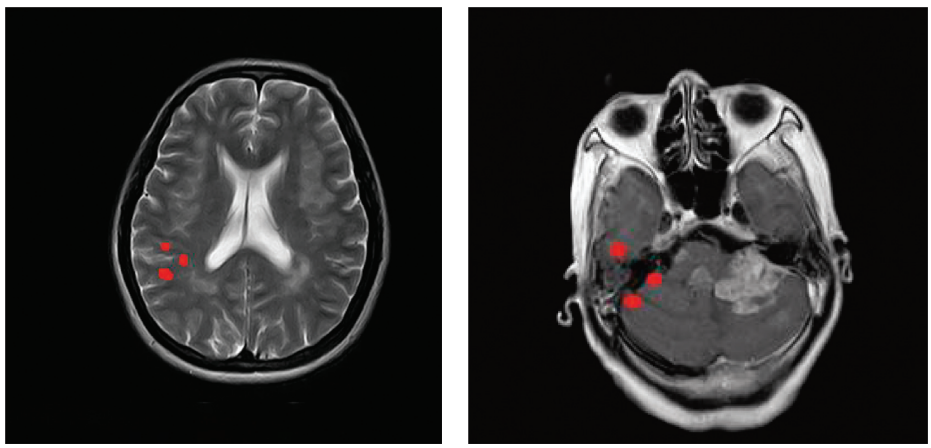

(a) (b)

Figure 7: BOLD-fMRI before the treatment. (a) The brain area around the stroke area. (b) The stroke area located in the parietal lobe.

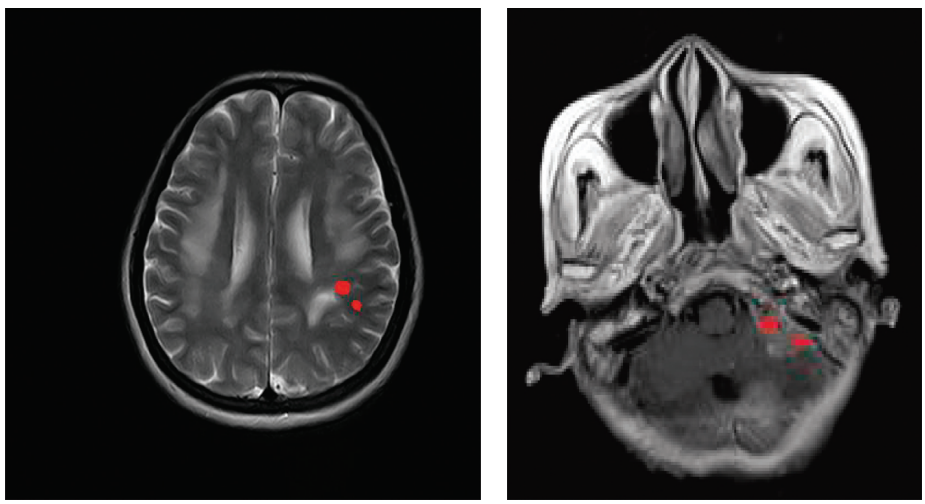

(a) (b)

Figure 8: BOLD-fMRI after the treatment. (a) Cerebral hemisphere excitation. (b) Sensorimotor cortex excitation.

activated brain areas for picture naming mainly included the right visual cortex, left fusiform gyrus, and left Broca, indicating that the picture naming mainly activated bilateral occipital lobes in the visual cortex, which was consistent with the results of Tan et al. [24].

When CIS patients performed finger exercise, the sensory motor areas on both sides were significantly activated, and the activated sensory motor areas on both sides were significantly bigger than the ipsilateral area. The activation rate of the left-sensory motor area (L-SM1) was 87.5%, the activation rate of the right-sensory motor area (R-SM1) was 25%, the activation rate of the left-side auxiliary motor area (L-SMA) was 62.5%, and the activation rate of the right-side auxiliary motor area (R-SMA) was 37.5%. It may be because of the functional impairment of the affected hemisphere in the acute phase. When the relevant brain functional areas in the affected brain hemisphere are activated, the patient's motor coordination will be impaired.

5. Conclusion

In the study, MCRSVMC algorithm was applied to process BOLD-fMRI images of CIA patients, and its performance was compared with that of random forest and SVM. The MCRSVMC algorithm proposed in this study was highly efficient and stable, and BOLD-fMRI diagnosis of motor function in CIS patients was mainly related to compensation around the lesion, which occurred on the healthy side after recovery. The limitation of this study is that the number of cases is small, which will reduce the power of the study. In the follow-up, an expanded sample size is necessary to strengthen the findings of the study. In conclusion, the changes of various brain function areas can be observed in real time through BOLD-fMRI images, providing an evidence-based basis for clinical diagnosis.

Data Availability

The data used to support the findings of this study are available from the corresponding author upon request.

Conflicts of Interest

The authors declare that they have no conflicts of interest.

References

[1] C. D. Maida, R. L. Norrito, M. Daidone, A. Tuttolomondo, and A. Pinto, "Neuroinflammatory mechanisms in ischemic stroke: focus on cardioembolic stroke, background, and therapeutic approaches," *International Journal of Molecular Sciences*, vol. 21, no. 18, p. 6454, 2020.

[2] R. Dhar, "Automated quantitative assessment of cerebral edema after ischemic stroke using CSF volumetrics," *Neuroscience Letters*, vol. 724, Article ID 134879, 2020.

[3] H. Du, D. Wilson, G. Ambler et al., "Clinical relevance of microbleeds in stroke (CROMIS-2) collaborators. Small vessel disease and ischemic stroke risk during anticoagulation for atrial fibrillation after cerebral ischemia," *Stroke*, vol. 52, no. 1, pp. 91–99, 2021.

[4] S. Paul and E. Candelario-Jalil, "Emerging neuroprotective strategies for the treatment of ischemic stroke: an overview of clinical and preclinical studies," *Experimental Neurology*, vol. 335, Article ID 113518, 2021.

[5] X. T. Su, L. Wang, S. M. Ma et al., "Mechanisms of acupuncture in the regulation of oxidative stress in treating ischemic stroke," *Oxidative medicine and cellular longevity*, vol. 2020, Article ID 7875396, 2020.

[6] G. Saliou, X. d'Ablon, M. Théaudin, T. Saliou, and S. Bourassi, "Cerebral computed tomography scan demonstrating ischemic stroke in a filly after intravenous antibiotic administration," *Journal of Equine Veterinary Science*, vol. 88, Article ID 102953, 2020.

[7] J. Lv, W. Guan, Q. You et al., "RIPC provides neuroprotection against ischemic stroke by suppressing apoptosis via the mitochondrial pathway," *Scientific Reports*, vol. 10, no. 1, p. 5361, 2020.

[8] P. P. W. Chu, A. M. Golestani, J. B. Kwinta, Y. B. Khatamian, and J. J. Chen, "Characterizing the modulation of resting-state fMRI metrics by baseline physiology," *NeuroImage*, vol. 173, pp. 72–87, 2018.

[9] A. Chakhoyan, A. Corroyer-Dulmont, M. M. Leblond et al., "Carbogen-induced increases in tumor oxygenation depend on the vascular status of the tumor: a multiparametric MRI study in two rat glioblastoma models," *Journal of Cerebral Blood Flow and Metabolism*, vol. 37, no. 6, pp. 2270–2282, 2017.

[10] C. Guo, J. Lu, Z. Tian, W. Guo, and A. Darvishan, "Optimization of critical parameters of PEM fuel cell using TLBO-DE based on Elman neural network," *Energy Conversion and Management*, vol. 183, no. MAR., pp. 149–158, 2019.

[11] M. Pruijm, B. Milani, and M. Burnier, "Blood oxygenation level-dependent MRI to assess renal oxygenation in renal diseases: progresses and challenges," *Frontiers in Physiology*, vol. 7, p. 667, 2017.

[12] Y. Chen, S. Hu, H. Mao, W. Deng, and X. Gao, "Application of the best evacuation model of deep learning in the design of public structures," *Image and Vision Computing*, vol. 102, Article ID 103975, 2020.

[13] M. Havlicek, A. Roebroeck, K. J. Friston, A. Gardumi, D. Ivanov, and K. Uludag, "On the importance of modeling fMRI transients when estimating effective connectivity: a dynamic causal modeling study using ASL data," *NeuroImage*, vol. 155, pp. 217–233, 2017.

[14] X.-a. Bi, Q. Shu, Q. Sun, and Q. Xu, "Random support vector machine cluster analysis of resting-state fMRI in Alzheimer's disease," *PLoS One*, vol. 13, no. 3, Article ID e0194479, 2018.

[15] X.-a. Bi, Q. Xu, X. Luo, Q. Sun, and Z. Wang, "Weighted random support vector machine clusters analysis of resting-state fMRI in mild cognitive impairment," *Frontiers in Psychiatry*, vol. 9, p. 340, 2018.

[16] J. Zhang and L. Chen, "Clustering-based undersampling with random over sampling examples and support vector machine for imbalanced classification of breast cancer diagnosis," *Computer Assisted Surgery*, vol. 24, no. 2, pp. 62–72, 2019.

[17] X.-a. Bi, Y. Wang, Q. Shu, Q. Sun, and Q. Xu, "Classification of autism spectrum disorder using random support vector machine cluster," *Frontiers in Genetics*, vol. 9, p. 18, 2018.

[18] X.-a. Bi, Q. Xu, X. Luo, Q. Sun, and Z. Wang, "Analysis of progression toward alzheimer's disease based on evolutionary weighted random support vector machine cluster," *Frontiers in Neuroscience*, vol. 12, p. 716, 2018.

[19] Y. Wang, H.-Y. Huang, Z.-T. Zuo, and Y.-Z. Wang, "Comprehensive quality assessment of Dendrubium officinale using

ATR-FTIR spectroscopy combined with random forest and support vector machine regression," *Spectrochimica Acta Part A: Molecular and Biomolecular Spectroscopy*, vol. 205, pp. 637–648, 2018.

[20] X. Gao and J. Cai, "Optimization analysis of urban function regional planning based on big data and GIS Technology," *Boletin Tecnico/Technical Bulletin*, vol. 55, no. 11, pp. 344–351, 2017.

[21] S. Pei, R. Dong, Y. Bao, R. L. He, and S. S.-T. Yau, "Classification of genomic components and prediction of genes of Begomovirus based on subsequence natural vector and support vector machine," *PeerJ*, vol. 8, Article ID e9625, 2020.

[22] Y. Zhang, Q. Deng, W. Liang, and X. Zou, "An efficient feature selection strategy based on multiple support vector machine technology with gene expression data," *BioMed Research International*, vol. 2018, Article ID 7538204, 2018.

[23] R. Pires, T. Falcari, A. B. Campo, B. C. Pulcineli, J. Hamill, and U. F. Ervilha, "Using a support-vector machine algorithm to classify lower extremity EMG signals during running shod/unshod with different foot strike patterns," *Journal of Applied Biomechanics*, vol. 26, pp. 1–15, 2018.

[24] Q. Tan, W. Li, and X. Chen, "Identification the source of fecal contamination for geographically unassociated samples with a statistical classification model based on support vector machine," *Journal of Hazardous Materials*, vol. 407, Article ID 124821, 2021.